

Synthesis and electropolymerisation of 3',4'-bis(alkylsulfanyl)terthiophenes and the significance of the fused dithiin ring in 2,5-dithienyl-3,4-ethylenedithiophene (DT-EDTT)

Cristina Pozo-Gonzalo,^a Tahir Khan,^a Joseph J. W. McDouall,^a Peter J. Skabara,^{*a} Donna M. Roberts,^b Mark E. Light,^c Simon J. Coles,^c Michael B. Hursthouse,^c Helmut Neugebauer,^d Antonio Cravino^d and N. Serdar Sariciftci^d

^aDepartment of Chemistry, University of Manchester, Oxford Road, Manchester, UK M13 9PL. E-mail: peter.skabara@man.ac.uk

^bMaterials Research Institute, Sheffield Hallam University, Sheffield, UK S1 1WB

^cDepartment of Chemistry, University of Southampton, Southampton, UK SO17 1BJ

^dLinz Institute for Organic Solar Cells (LIOS), Physical Chemistry, Johannes Kepler University Linz, Linz A-4040, Austria

Received 4th October 2001, Accepted 6th December 2001

First published as an Advance Article on the web 31st January 2002

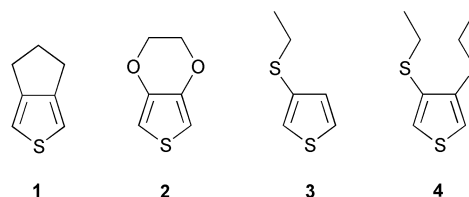
A new series of regioregular poly(terthiophenes), bearing bis(thioether) side groups, has been prepared by electrochemical oxidation. Cyclic voltammetry of the parent trimers reveals an increase in electron donating ability in cyclic thioether derivatives. For example, one compound containing a central ethylenedithiophene (EDTT) unit gives two irreversible oxidation peaks which are significantly lower than the corresponding values for the structurally analogous bis(methylthio) derivative ($\Delta E_{1ox} = 170$ mV, $\Delta E_{2ox} = 30$ mV). The difference in oxidation potentials of each terthiophene in acetonitrile solution can be explained by examining the highest occupied molecular orbital (HOMO) energies. The electrochemical behaviour of the polymers illustrates the increase in p-doping ability of the EDTT-containing polymer. The cyclic voltammograms and electronic absorption spectra of the polymers show that the polymers containing cyclic thioether units have the lowest bandgap in the series (*ca.* 1.4 V and 1.5 eV, respectively). Photoinduced IR spectroscopy of poly(dithienyl-3,4-ethylenedithiophene) provides evidence of a long-living photoexcited charged state in the polymer.

Introduction

The strategy of attaching substituents onto the backbone of poly(thiophene) (PT) is essential in order to overcome the low solubility and hence poor processability of the parent polymer PT. However, these side-chains usually impart a change in the material's properties other than an improvement in solubility, which is either part of the design of the polymer¹ or is typically consequential. The incorporation of simple linear alkyl side-groups is a good example. Polymers derived from 3-methylthiophenes have shown improved conjugation and conductivity due to the effect of reducing α - β' couplings;² furthermore, the methyl groups have a small inductive effect, which causes a decrease in the oxidation potential of the material. Very recently it has been shown that poly(3-hexylthiophene) becomes superconducting below 2.4 K, due to the self-organisation of the polymer into a highly ordered structure.³ However, there is also a trade-off in the case of alkyl substituents: steric hindrance, predominantly between head-to-head dimer units, causes the thiophene rings to be forced out of coplanarity, resulting in poor π -orbital overlap and hence a decrease in the level of conjugation in the chain. This effect is inflated in 3,4-dialkyl substituted thiophenes, in which α - α' couplings are exclusive: lower conductivities and higher optical bandgaps and oxidation potentials have been noted in disubstituted polymers compared with monosubstituted analogues.⁴ Cyclisation of the 3,4-positions, for example in dihydrocyclopenta[*c*]thiophene (**1**), reduces steric hindrance to some degree, although the all-round electronic properties of the polymer are still inferior to those of poly(3-methylthiophene).⁵

Alkoxy-substituted thiophenes benefit from a larger electron donating effect through a π -resonance contribution from the oxygen atoms. Hence, poly(3-alkoxythiophene)s have smaller optical bandgaps and lower oxidation potentials than poly(alkylthiophene)s, yet, because of a higher level of steric hindrance, the conductivity of the former is much poorer than the latter.⁴ This loss in conductivity is perpetuated in poly(bis(alkoxy)thiophene)s; however, cyclisation of the ether units in the case of poly(ethylenedioxythiophene) (PEDOT, **2**) has provided a material with surprisingly interesting electronic and conducting properties.⁶

Work reported on polymers derived from alkylthio substituted thiophenes,⁷⁻¹³ has shown similar trends as for alkoxythiophenes, but the electropolymerisation of these thioether compounds can prove difficult. For example, theoretical calculations have shown that the electron spin density distribution in radical cations of alkylsulfanyl derivatives **3** and **4** is not favorable for α - α' coupling.¹⁰ Nevertheless, poly(thiophene)s bearing conjugated sulfur-containing side-groups are still desirable targets, since any intermolecular S...S attractions could promote electronic interaction between chains, which would in turn raise the level of charge mobility



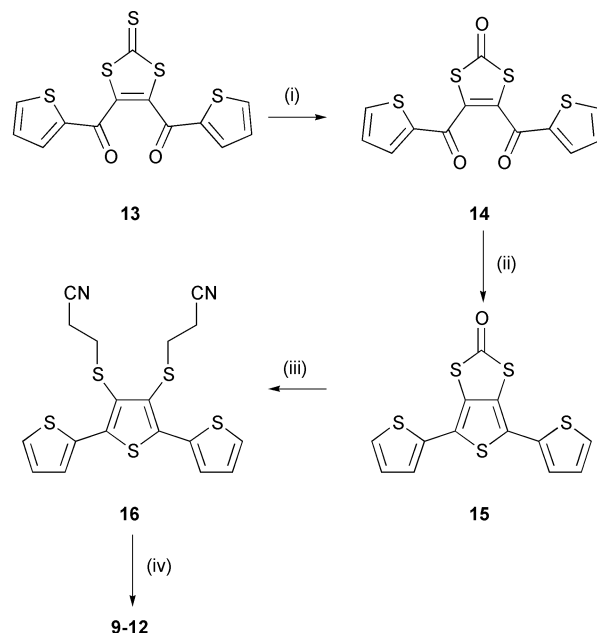
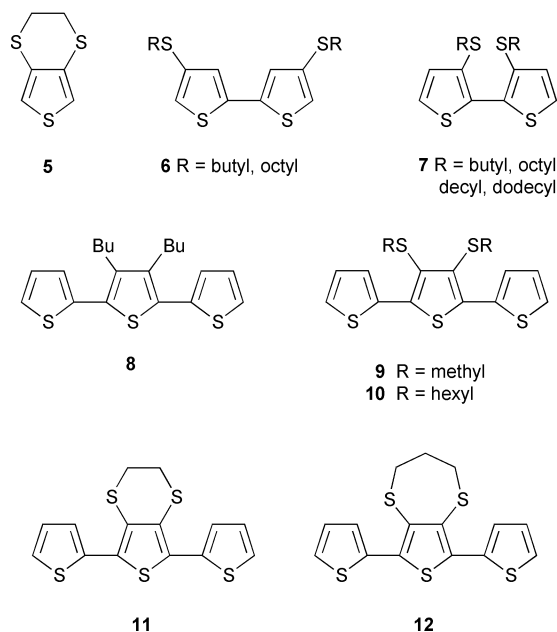
in the bulk material. A landmark in this field has been the preparation of the sulfur analogue of PEDOT: 3,4-ethylenedithiothiophene (**5**).¹⁴ Monomer **5** undergoes facile polymerisation by chemical or electrochemical oxidation, to give a stable polymer with a conductivity of 0.1–0.4 S cm⁻¹, but to date there has only been one paper published on this material, which is in stark contrast to the well-studied EDOT system.^{15–24} Further examples of electropolymerisable alkylsulfanyl thiophenes include the bithiophenes **6**²⁵ and **7**.²⁶ Poly(**6**) and poly(**7**) represent head-to-head/tail-to-tail polymers, which have shown improved electroactive properties compared to analogous alkyl derivatives.

In order to counteract the trade-off observed in 3,4-disubstituted poly(thiophenes) (*i.e.* a positive contribution towards lowering the bandgap and oxidation potential *vs.* steric hindrance and low conductivity), one useful strategy involves the incorporation of the substituted thiophene species into a terthiophene unit. Hence, the steric effect of the substituents is diluted in the resulting polymer, since the side-chain fragments will be adjacent to unsubstituted thiophene rings. One notable example includes the dibutyl substituted poly(terthiophene) **8**.²⁷ Following this design strategy, we have prepared the 3',4'-bis(alkylsulfanyl)terthiophenes **9–12**; herein, we report on the synthesis and electrochemical polymerisation of these materials, which are rare examples of terthiophenes bearing bis(alkylsulfanyl) substituents on the central ring.²⁸

Results

Synthesis

The preparation of terthiophenes **9–12** is illustrated in Scheme 1. Diketone **13**²⁹ was treated with mercury(II) acetate to afford the carbonyl analogue **14** in 76% yield. Conversion of **14** to the terthiophene derivative **15** (63%) was achieved by heating a dioxane solution of the starting material to 90 °C in the presence of phosphorus pentasulfide and sodium bicarbonate. The reaction of potassium *tert*-butoxide with **15**, followed by the addition of two equivalents of 3-bromopropionitrile, gave the bis(cyanoethylsulfanyl) derivative **16** in 70% yield. Finally, sequential treatment of compound **16** with tetrabutylammonium hydroxide and the appropriate alkyl halide gave terthiophenes **9–12** in 52–68% yield. The preparation of bis(alkylthio) terthiophenes **9–12** directly from **15** was attempted, but the yields proved to be inferior to those achieved *via* Scheme 1.



Scheme 1 Reagents and conditions: (i) Hg(OAc)₂, CHCl₃–AcOH (3 : 1), rt; (ii) P₂S₅, NaHCO₃, 1,4-dioxane, 90 °C; (iii) Bu^tOK, THF, 0 °C, then 3-bromopropionitrile; (iv) n-Bu₄NOH, THF, 0 °C, then methyl iodide, hexyl bromide, 1,2-dibromoethane or 1,3-dibromopropane.

X-Ray crystallography

Slow evaporation of a dichloromethane solution of compound **11** afforded yellow crystals which were submitted for X-ray crystallography.³⁰ The asymmetric unit is labelled in Fig. 1, which identifies a mirror plane bisecting the S(2) atom and the C(7)–C'(7) bond. The disorder prevalent within the saturated alkyl fragment is quite common for ethylenedithio units in 2,3-dihydro-1,4-dithiin species.³¹ Two conformations of the C₄S₂ ring were refined, each with a 50% occupancy. There is a close intramolecular S··S contact between S(1) and S(2) atoms (3.33 Å), significantly shorter than the sum of the van der Waals radii for two sulfur atoms (3.60 Å). Surprisingly, the molecule adopts an all-*syn* conformation. The torsion angle between the peripheral and central thiophene rings is –140.6° [C(6)–C(5)–C(4)–S(1)]. A search for terthiophene systems was made using the Cambridge Crystallographic Database.³² The X-ray crystal structures of 13 terthiophene species have been reported,^{33–41} however, none of these bear the all-*syn* conformation.

Compound **12** was recrystallised from dichloromethane–petroleum ether to afford orange crystalline blocks. The X-ray crystal structure of **12**⁴² is shown in Fig. 2, revealing an all-*anti* conformation; however, one peripheral thiophene ring [C(7)–S(4)–C(8)–C(9)–C(10)] is distorted between *syn* and *anti* conformers. Close intramolecular S··S contacts exist between

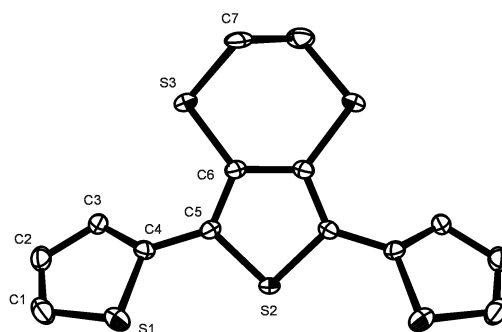


Fig. 1 The asymmetric unit of compound **11** showing the all-*syn* conformation of the terthiophene unit (H-atoms have been excluded and the disorder in the C(7)–C'(7) bond has not been shown).

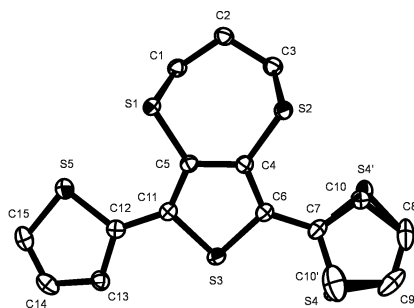


Fig. 2 X-Ray crystal structure of compound 12.

S(5)–S(1) (3.232 Å) and S'(4)–S(2) (3.279 Å) atoms. These interactions assist in the planarisation of the terthiophene unit, giving torsion angles of 167.28° [S(5)–C(12)–C(11)–S(3)] and –157.54° [C(4)–C(6)–C(7)–S(4)] or –153.97° [S(3)–C(6)–C(7)–S'(4)].

Electrochemistry

The cyclic voltammograms for compounds 9–12 are shown in Fig. 3. All four terthiophenes give two irreversible oxidation peaks (Table 1), however, the ethylenedithio derivative 11 proves to be the strongest electron donor. There is little discrepancy between the first oxidation potentials of 9, 10 and 12 (+1.16, +1.17 and +1.13 V, respectively), but E_{1ox} for 11 is shifted to a lower value by *ca.* 170 mV. The values for the second oxidation potential for 9, 11 and 12 are roughly equal (+1.66, +1.63 and +1.67 V, respectively), whilst E_{2ox} for 10 is somewhat higher at +1.79 V. Since the inductive electronic effect of the substituents will be approximately the same for all four derivatives, the most remarkable difference in electrochemical behaviour is between compounds 9 and 11. Although these two terthiophenes are almost structurally identical, there is an obvious discrepancy between their first oxidation potentials. This could be due to the minimisation of steric repulsion between the ethylenedithio fragment and the neighbouring thiophene rings, which enhances the donor abilities of 11. In contrast, for derivative 9 there is free rotation around the C3'–S and C4'–S bonds which deters the triaryl unit from a coplanar conformation. The structural arrangement of 11 in Fig. 1 cannot be invoked to contradict this prediction, since the electroactivity of the terthiophene species is studied in solution state. However, in terthiophene 12 rotation is also restricted for the C3'–S and C4'–S bonds, yet the first oxidation potential is still 140 mV higher than the corresponding value for the ethylene analogue 11. In order to explain the trend in oxidation potentials, we performed a series of calculations relating the different conformers of compounds 9, 11 and 12 with experimental results.

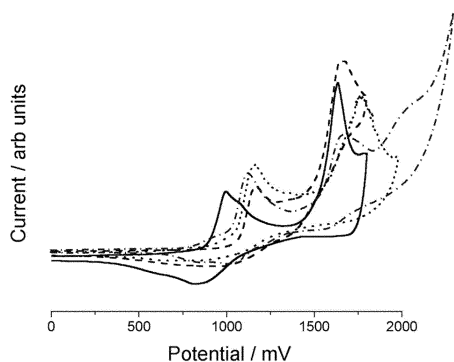


Fig. 3 Cyclic voltammograms of terthiophenes 9 (---), 10 (···), 11 (—) and 12 (— · —) in acetonitrile, Au working electrode, aqueous Ag/AgCl reference electrode, 0.1 M *n*-Bu₄NPF₆ supporting electrolyte, *ca.* 10^{–3} M substrate, scan rate 100 mV s^{–1}.

Table 1 Cyclic voltammetry and absorption spectroscopy data for monomers 9–12, poly(9), poly(10), poly(11) and poly(12)

Monomers	9	10	11	12
E_{1ox}/V^a	+1.16 ^e	+1.17 ^e	+0.99 ^e	+1.13 ^e
E_{2ox}/V^a	+1.66 ^e	+1.79 ^e	+1.63 ^e	+1.67 ^e
λ_{max}/nm^b	360	368	368	375
Polymers				
r^c	0.9994	0.9993	0.9959	0.9988
Redox peaks/V ^a	+1.22, –1.10 ^e	+1.20, –1.15 ^e	+0.64, +0.99, –1.39 ^e	+1.08, –1.12 ^e , –1.31
λ_{max}/nm^d	487	489	478	487
Optical bandgap/eV	(1.58)	1.97	1.53	1.45
Electrochemical bandgap/V ^{ad}	1.54	1.61	1.44	1.43

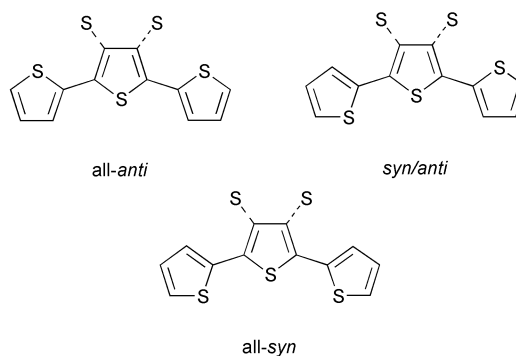
^aIn acetonitrile. ^bIn dichloromethane. ^cCorrelation coefficient from Fig. 7. ^dAs a film on ITO glass. ^eIrreversible peak.

Computational results

All calculations were performed using the GAUSSIAN 98 suite of programs.⁴³ Starting geometries for the terthiophenes, 9, 11 and 12, with the ring sulfur atoms in all-*anti*, *syn/anti* and all-*syn* conformations (Scheme 2) were obtained using the PM3 model. These geometries were then fully optimised at the B3LYP/6-31G(d,p) level of theory. Solvent effects were included (using gas phase geometries) by employing the polarisable continuum model (PCM) using acetonitrile as solvent ($\epsilon = 36.64$).

Table 2 shows the relative conformational stabilities of the neutral and cation forms of 9, 11 and 12. For 9, it is found that the *trans* orientation of the two methylthio groups gives lower energies than the *cis* orientation. The lowest energy conformations for both the neutral and cationic forms of 9, in the gas phase and acetonitrile, are predicted to be *trans* all-*anti*. For neutral 11, the most stable structure is calculated to be the all-*syn* conformer, in agreement with the crystallographic results. However, the cation form of 11 shows a preference for the all-*anti* conformation. The differences in energy are small and the all-*anti* conformation of neutral 11 should be accessible in acetonitrile and the gas phase. Compound 12 also shows a preference for the all-*anti* conformation.

Table 3 compares theoretical and experimental values with some of the key geometrical parameters. The calculated structures show a slight asymmetry in the geometries, hence when two values are indicated for a parameter, they refer to different sides of the central ring. It can be seen that the calculated bond lengths are in reasonable agreement with the available X-ray structures. The torsion angles are less well reproduced, but it should be borne in mind that torsion angles will have much softer potentials than the bond lengths and will be subject to



Scheme 2

Table 2 Calculated (B3LYP/6-31G(d,p)) relative stabilities (kJ mol⁻¹) of conformers of **9**, **11** and **12**

Structure	Neutral		Cation	
	Gas phase	Acetonitrile	Gas phase	Acetonitrile
9				
<i>cis</i> all- <i>anti</i>	0.0	0.0	0.0	0.0
<i>cis</i> <i>syn/anti</i>	0.1	1.5	2.1	15.4
<i>cis</i> all- <i>syn</i>	1.9	5.2	6.3	5.9
<i>trans</i> all- <i>anti</i>	-6.1	-4.2	-8.3	-5.9
<i>trans</i> <i>syn/anti</i>	-2.4	0.4	-2.4	17.2
<i>trans</i> all- <i>syn</i>	-2.6	2.6	11.1	3.4
11				
all- <i>anti</i>	0.0	0.0	0.0	0.0
<i>syn/anti</i>	-2.8	-1.9	1.8	4.2
all- <i>syn</i>	-3.9	-2.4	5.7	9.6
12				
all- <i>anti</i>	0.0	0.0	0.0	0.0
<i>syn/anti</i>	3.8	4.2	5.3	6.7
all- <i>syn</i>	1.2	4.5	10.6	15.0

more fluctuation. The agreement between theoretical and X-ray torsion angles is worst for **12**, but the X-ray structure shows a good deal of disorder and so the result is reasonable.

The calculated gas and solution phase ionisation potentials, together with the experimental oxidation potentials, are shown in Table 4. Solvation reduces the energy required to form the cation by a significant amount. This is due to a positive $\Delta G_{\text{solvation}}$ for the neutral and a negative $\Delta G_{\text{solvation}}$ for the cation in all cases.

The absolute values of the calculated solution phase ionisation potentials cannot be compared directly with the experimental values obtained by cyclic voltammetry. This is because the free energy associated with the reference electrode (silver/silver chloride) must be included and the systems must be referred to the same standard states. However, a plot of the calculated potentials against the experimental values gives a straight line with a correlation coefficient of 0.971. In comparing with experiment we have chosen the oxidation potential corresponding to the all-*anti* conformation of **11**. This is 120 mV lower than the oxidation potential for the all-*syn*

Table 3 Comparison of X-ray and theoretical values of key geometrical parameters (bond lengths in Å, angles in °). See Fig. 1 and 2 for atom numbering

Structure	Parameter	X-Ray	B3LYP/6-31G(d,p)
11 all- <i>syn</i>	S(1)–S(2)	3.33	3.364, 3.385
	C(6)–C(5)–C(4)–S(1)	-140.6	-141.84, -142.35
	S(1)–S(2)–C(6)–C(5)–C(4)–S(1)		3.347, 3.341 -139.93, -143.148
12	S(5)–S(1)	3.232	3.295
	S'(4)–S(2)	3.279	3.287, 3.288
	C(4)–C(6)–C(7)–S(4)	-157.54	-146.44
	S(3)–C(6)–C(7)–S'(4)	-153.97	-161.70, -161.58
	S–S(Me)		3.230, 3.231
9 all <i>anti</i>	S(ring)–C–C–S(ring)		177.34, 176.28

Table 4 Calculated (B3LYP/6-31G(d,p)+PCM) ionisation and experimental oxidation potentials of compounds **9**, **11** and **12**

	Ionisation potential (gas phase)/V	Ionisation potential (acetonitrile)/V	Oxidation potential (experiment)/V
9			
<i>cis</i> all- <i>anti</i>	6.49	5.19	1.16
<i>cis</i> <i>syn/anti</i>	6.51	5.33	
<i>cis</i> all- <i>syn</i>	6.54	5.20	
<i>trans</i> all- <i>anti</i>	6.47	5.17	
<i>trans</i> <i>syn/anti</i>	6.49	5.36	
<i>trans</i> all- <i>syn</i>	6.63	5.20	
11			
all- <i>anti</i>	6.26	4.97	0.99
<i>syn/anti</i>	6.31	5.03	
all- <i>syn</i>	6.36	5.09	
12			
all- <i>anti</i>	6.36	5.09	1.13
<i>syn/anti</i>	6.37	5.11	
all- <i>syn</i>	6.45	5.20	

conformer. Recalling the previous discussion about the conformers of **11**, this is justified.

Experimentally the relative oxidation potentials are **11** (0.00 V) < **12** (0.14 V) < **9** (0.17 V). The calculated ionisation potentials reproduce the trend with reasonable accuracy, giving **11** (0.00 V) < **12** (0.12 V) < **9** (0.21 V). The difference in calculated ionisation potential between **11** and **9** is approximately 20 kJ mol⁻¹. This energetic difference can be understood by inspection of the highest occupied molecular orbital (HOMO) of each structure in acetonitrile. The HOMO is the orbital from which an electron must be ejected to form the cation. Looking at the plots of HOMO (Fig. 4) it can be seen that for **11** the p-orbitals on the sulfur atoms of the thioether moieties are aligned parallel with π -orbitals of the central thiophene ring and are in an antibonding arrangement. In **12**, the thioether sulfur p-orbitals are rotated somewhat with respect to the plane of the central thiophene ring, allowing a bonding interaction. This stabilises the HOMO, as evidenced by the lowering of the orbital energy, making ionisation of **12** more difficult than that of **11**. In the HOMO of **9**, the thioether sulfur p-orbitals are aligned along the S–Me bond and well removed from interaction with the central ring π -orbitals. Since this interaction is antibonding, this also serves to stabilise the HOMO. A plot of the HOMO energies against the experimental oxidation potentials gives a straight line with a correlation coefficient of -0.981. A similar plot of the gas phase HOMO energies gives a very poor correlation coefficient of -0.719, indicating the importance of the solvent. Clearly the stability of the HOMO is a key factor in determining the electrochemistry of the terthiophenes.

Electrochemical polymerisation

All four compounds **9–12** have been polymerised electrochemically on gold electrodes and ITO glass (in dichloromethane or acetonitrile), by repetitive scanning over the first (or both) oxidation waves. The corresponding voltammograms are shown in Fig. 5, which illustrates the electrodeposition of the polymers in acetonitrile. In all cases, the emergence of a new reversible redox wave is indicative of the formation (and electroactivity) of the corresponding polymer on the working

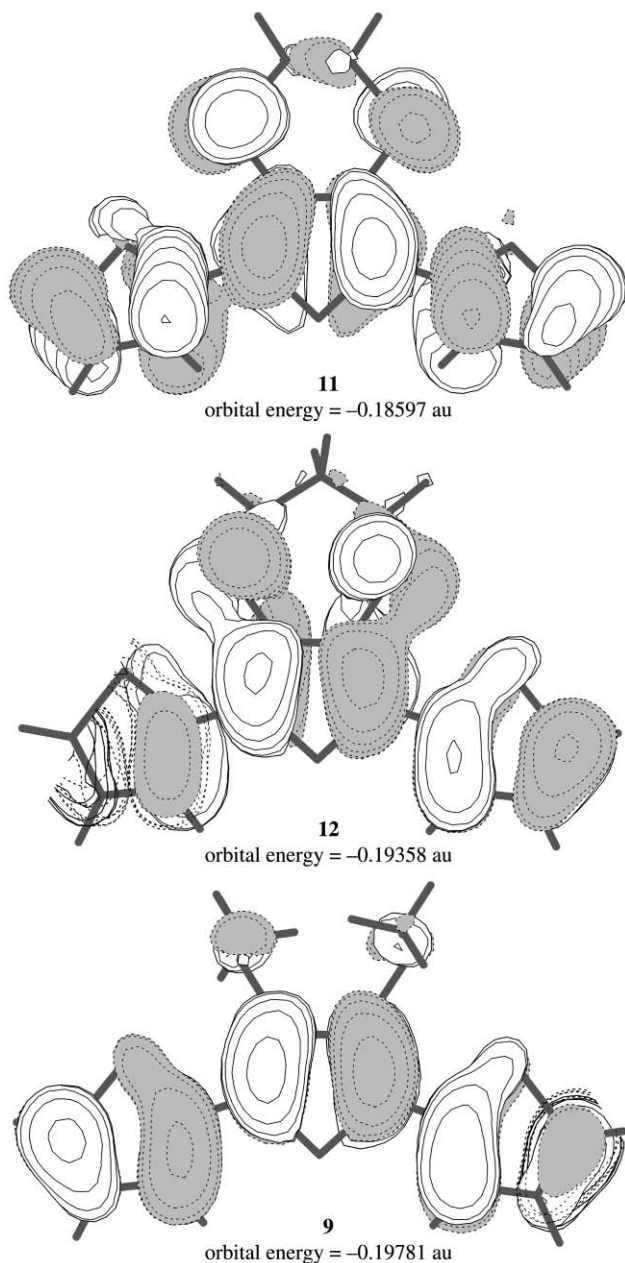


Fig. 4 Orbital energies and surface plots (0.02 au; 1 au (measured in hartree) $\equiv 4.35975 \times 10^{-18}$ J) of the HOMO orbitals of **9**, **11** and **12** in acetonitrile from B3LYP/6-31G(d,p)+PCM calculations.

electrode. Fig. 6 displays the cyclic voltammograms of poly(**9**) and poly(**11**) in monomer-free acetonitrile solution, and are representative for the electroactivity of the poly(bisalkylthio terthiophene) series. All four polymers were thoroughly dedoped before oxidation or reduction to eliminate the possibility of charge trapping between experiments. A single irreversible reduction peak is seen for all polymers between -1.10 V and -1.39 V (Table 1). For poly(**9**) and poly(**10**), a single broad reversible oxidation peak is seen at $+1.22$ and $+1.20$ V, respectively. The corresponding redox wave for poly(**12**) is shifted to a less positive value of $+1.08$ V. Conversely, for poly(**11**), two oxidation waves are observed at $E_{1/2} = +0.64$ V and $E_{2/2} = +0.99$ V (quasi-reversible), proving that the polymer is a more efficient electron donor than the other related polythiophenes (*i.e.* an increased number of redox states at lower potentials). The linear relationship between the maximum peak current (in the range 0.0 V to $+1.5$ V) for E_{1ox} and the scan rate (25 – 500 mV s^{-1}) for poly(**9**), poly(**10**), poly(**11**) and poly(**12**) can be seen in Fig. 7. The behaviour is typical of an electroactive polymer attached to an electrode

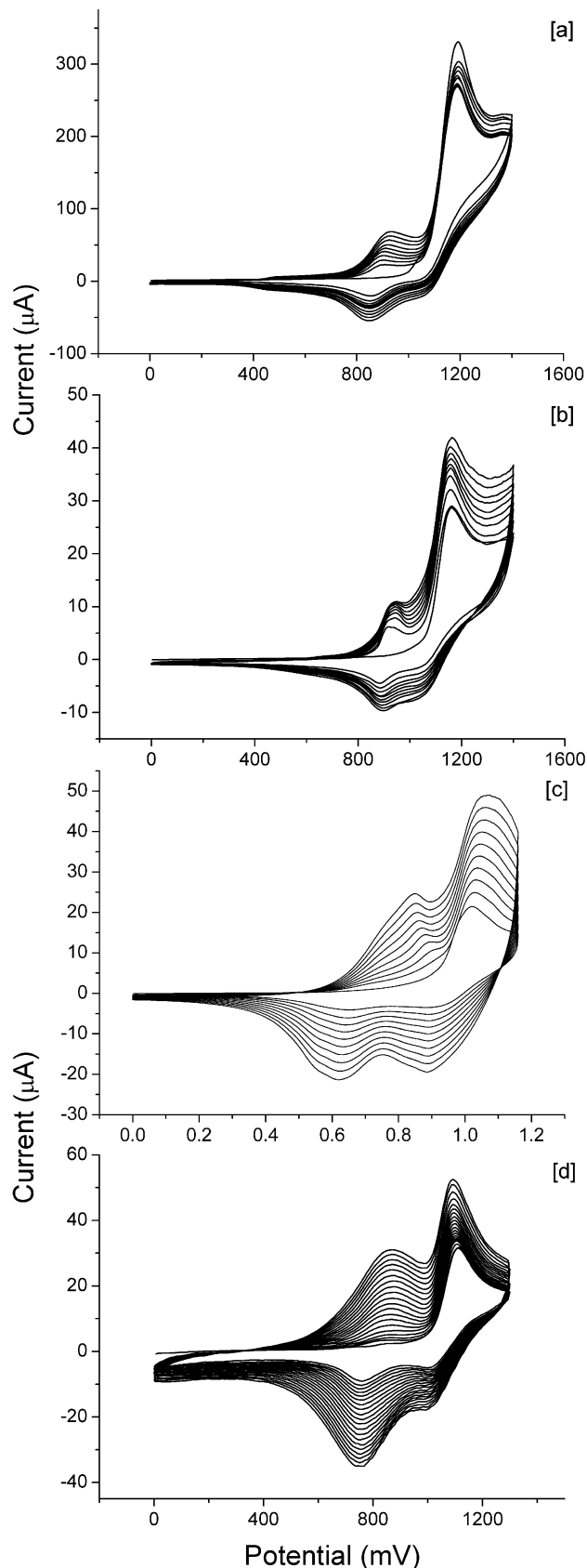


Fig. 5 Electrodeposition of (a) poly(**9**) (on ITO glass, 100 mV s^{-1}), (b) poly(**10**) (on Au disk, 100 mV s^{-1}) and (d) poly(**12**) (on Au disk, 100 mV s^{-1}), Ag/AgCl reference electrode, 0.1 M $n\text{-Bu}_4\text{NPF}_6$ supporting electrolyte, *ca.* 10^{-3} M substrate in acetonitrile.

surface; all four fits possess a high correlation coefficient (r , Table 1), which exemplifies the stability of the polymers towards p-doping up to $+1.5$ V. The difference between the

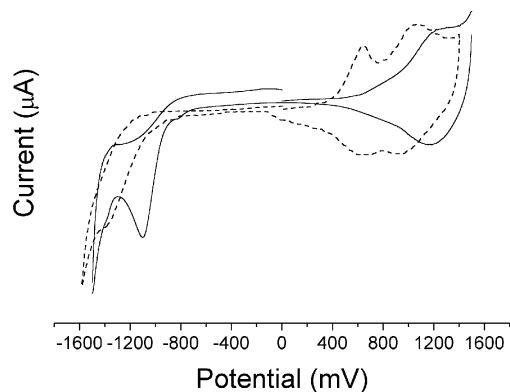


Fig. 6 Cyclic voltammograms of poly(9) (—) deposited on Au disk and poly(11) (- - -) deposited on ITO glass, monomer-free acetonitrile, aqueous Ag/AgCl reference electrode, 0.1 M *n*-Bu₄NPF₆ supporting electrolyte.

onset potentials for the reduction process and $E_{1ox}^{1/2}$ represents the electrochemical bandgap (E_g); thus, values of 1.54, 1.61, 1.44 and 1.43 V were measured for poly(9), poly(10), poly(11) and poly(12) respectively. It is noteworthy that the bandgap values were lowest for the ethylene and propylene containing polymers, poly(11) and poly(12).

FTIR spectroscopy: *in situ* spectroelectrochemistry and photoinduced absorption.

Molecules with extended delocalised π -electron systems usually exhibit a strong coupling between electronic and vibrational properties. Because of such electron–phonon coupling, infrared spectroscopy on conjugated polymers not only gives geometrical but also electronic information.⁴⁴ In particular, the IR spectra of conjugated polymers in their oxidised (reduced) or photoexcited, conducting forms are characterised by dramatic changes, compared to the spectra of the pristine semiconducting form, due to new electronic transitions involving *intragap* electronic states and infrared active vibrations (IRAV).^{44,45} The characteristics of these spectral features correlate to the effective conjugation length of the macromolecule and thus to the delocalisation of the radical-ions (widely accepted to be polarons) formed on the polymer by the chemical or photoinduced redox process.^{44–46} The rather small bandgap observed for poly(11) makes it an interesting material for possible applications in optoelectronic devices (*e.g.* plastic solar cells⁴⁷). We have investigated the changes in the IR absorption spectrum of poly(11) due to electrochemical oxidation (Fig. 8) and photoexcitation (Fig. 9). The broad absorption feature

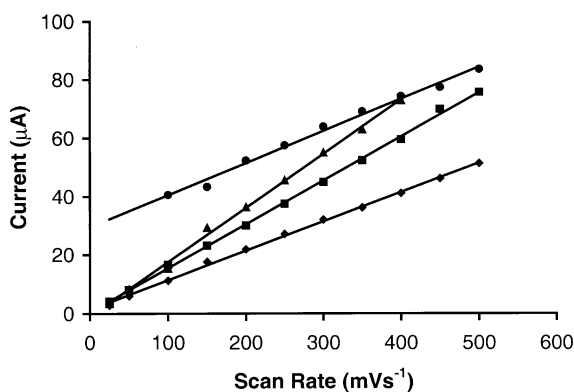


Fig. 7 Plots of scan rate ($mV s^{-1}$) vs maximum peak current of E_{1ox} (μA) for poly(9) [■], poly(10) [◆], poly(11) [●] and poly(12) [▲]. Experiments conducted in monomer-free acetonitrile, using an aqueous Ag/AgCl reference electrode, 0.1 M *n*-Bu₄NPF₆ supporting electrolyte; current for poly(11) has been scaled down by a factor of 10 for ease of comparison. Correlation coefficients are all >0.99.

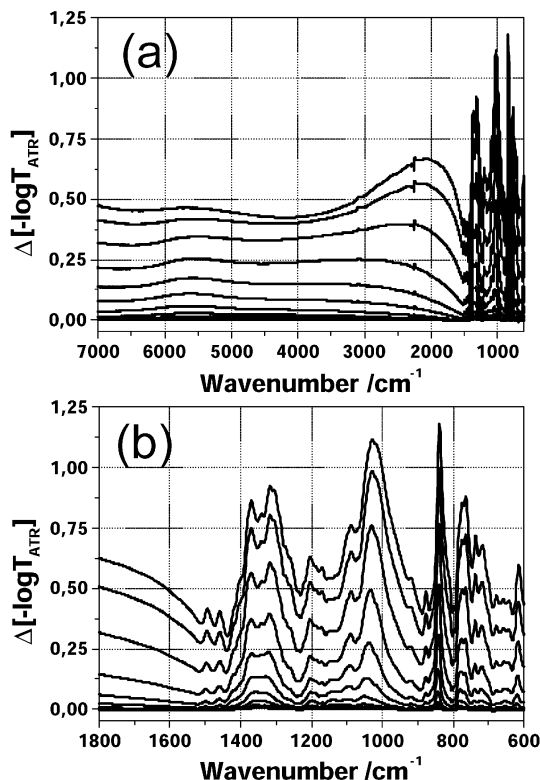


Fig. 8 Electrochemically induced IR absorption of poly(11) (room temperature). (a): full range; (b): IRAV range.

in the high frequency part of the spectrum in Fig. 8(a) ($1500\text{--}7000\text{ cm}^{-1}$, corresponding to 0.18–0.87 eV) is related to the *intragap* electronic transitions of the radical-cations formed during the oxidation. The maximum observed at higher energy (around 5560 cm^{-1}) evolves mainly during the first oxidation wave seen in the cyclic voltammogram of poly(11), up to

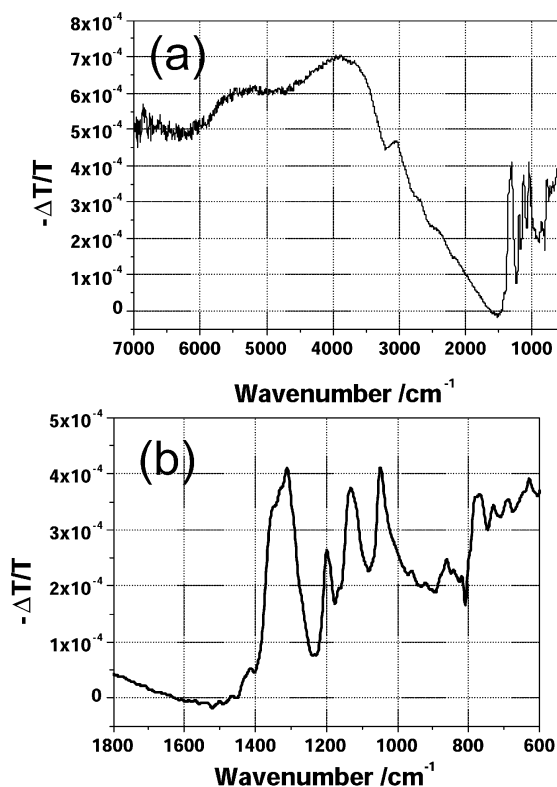


Fig. 9 Photoinduced IR absorption of poly(11) (100 K). Excitation at 488 nm; 22 mW cm^{-2} . (a): full range; (b): IRAV range.

electrode potentials of about 700 mV. The broad absorption feature at lower energy (around 3000 cm^{-1}) shows a pronounced maximum during the second oxidation process (redshifting to 2100 cm^{-1} with increasing electrode potential). Fig. 8(b) displays in detail the vibrational part of the spectrum. The most relevant IRAV bands of oxidised poly(**11**) are at about 1350 cm^{-1} (ω_1 , splitting in two bands at high potential), 1200 (ω_2), 1090 (ω_3), 1035 (ω_4) and 767 cm^{-1} (ω_5). Such a pattern is similar to those of polythiophenes.⁴⁴ On the other hand, a rather intense and narrow band is also seen at 615 cm^{-1} (ω_6), out of the range commonly discussed for IRAVs. A narrow IRAV band, assigned to a vibration containing C–S stretching character, has been observed at a similar wavenumber in polydithienothiophene pDTT3.⁴⁸ The analogous behaviour for the band at 615 cm^{-1} in the oxidised poly(**11**) IR spectrum, could be due to the π -resonance contribution of the two sulfur atoms within the alkylthio substituent. Note that the very sharp and intense band seen at 839 cm^{-1} is due to the incorporation of PF_6^- as counterions.

The photoinduced IR spectrum of poly(**11**) is depicted in Fig. 9. The simultaneous observation of one electronic band, with a maximum around 3900 cm^{-1} (Fig. 9(a)), and IRAV bands (Fig. 9(b)) clearly indicate the charged nature of long-living photoexcitations.^{44,45,49} Similar to some other photodoped conjugated polymers,^{48,50} IRAV bands do not show the expected shift towards lower wavenumbers as compared to the electrochemically doped materials.⁵¹ Conversely, for the bands ω_3 and ω_6 even a blue-shift (1132 and 628 cm^{-1} instead of 1090 and 615 cm^{-1}) is observed in the photodoped poly(**11**) spectrum. Although electrolyte counterions are absent, a kind of pinning, probably due to deeply trapped charged sites, occurs also in the photodoped polymer.

Electronic absorption spectroscopy

The absorption maxima in the UV/vis spectra of compounds **9–12** are similar ($360\text{--}375\text{ nm}$ in CH_2Cl_2 , Table 1). The longest wavelength maximum is obtained for compound **12** and is indicative of a higher degree of coplanarity in the terthiophene unit, compared to the remainder of the series. For polymer films deposited on ITO glass, the value of λ_{max} is in the range $478\text{--}489\text{ nm}$. The optical bandgaps of the polymers obtained by UV/vis spectroscopy of ITO deposited films are estimated from the longest wavelength absorption edge and are in the region $1.45\text{--}1.97\text{ eV}$ (Table 1). The spectra for all four polymers after dedoping are shown in Fig. 10. Although the absorption maxima for the poly(bisalkylthioterthiophene)s are similar, the ‘tail’ characteristics differ. The absorption edge for each of the fused ring containing polymers is several hundred nanometres

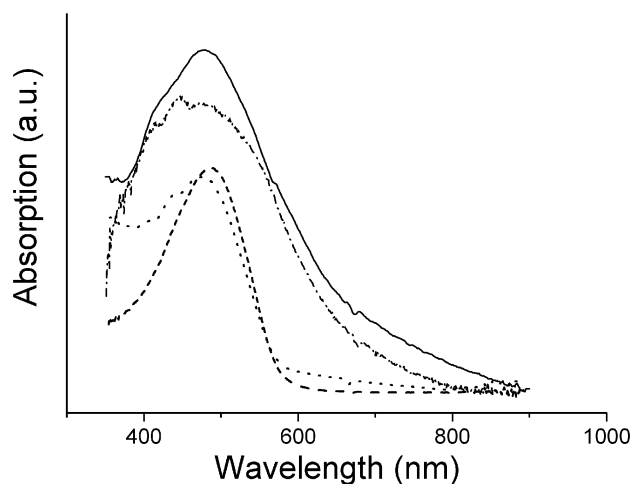


Fig. 10 Absorption spectra of poly(**9**) (·····), poly(**10**) (---), poly(**11**) (— · — · —) and poly(**12**) (—) deposited on ITO glass.

higher than the corresponding absorption maximum and the estimated bandgaps are close to those derived from cyclic voltammetry with the band edge lying in the NIR region of the spectrum. In the case of poly(**10**), however, the band edge is much closer to the absorption maximum, giving a value of 1.97 eV for the optical bandgap. Noticeably, there is a large discrepancy between the optical and electrochemical (1.61 V) bandgaps for poly(**10**). This may be due to the redox activity of localised sites in the material, namely the electron rich bis(alkylthio) thiophene units, rather than the oxidation/reduction behaviour of the delocalised conjugated chain. In the case of poly(**9**), the absorption maximum tail is apparent but very weak, making it difficult to conclude with confidence where exactly the band edge is situated.

Discussion

Understanding the physico-structural relationship of conjugated polymers requires the consideration of a number of criteria. According to Roncali,⁵² the bandgap of polyaromatic conjugated species is defined by five features of the polymer: (i) bond length alternation (BLA); (ii) the degree of planarity within the chain; (iii) the aromatic resonance energy of the ring system; (iv) the electronic push/pull effect of substituents; (v) contribution of intermolecular or interchain contacts in the solid state. Table 5 lists the calculated values for BLA, the longest wavelength absorption maxima and the torsion angles for compounds **9–12** and dimers **9₂**, **11₂** and **12₂**, corresponding to sexithiophene analogues.⁵³ Experimental values for BLA, torsion angles and absorption maxima are also given in Table 5. Each compound was optimised in the all-*anti* conformation, unless stated, and the calculated values are obtained from derivatives in the gaseous state. The degree of BLA decreased from **9** to **11**; since this is a measure of conjugation in the polyene chain, there is good agreement with the theoretical and experimental values for the longest wavelength absorption maximum, which also decrease from **9** to **11** for the all-*anti* conformers. The average value for the torsion angles increases in the series **9** to **11**, indicating that BLA must be the dominant factor in the determination of the longest wavelength absorption maximum. For compound **12**, the degree of BLA (0.027 \AA) is intermediate compared to the remainder of the terthiophenes, yet the coplanarity between rings is far less than in compounds **10** and **11**. This leads to an identical prediction for λ_{max} compared to the *anti* conformer in **11** (421 nm), yet the experimental value is higher in **12** (375 nm) than the former (368 nm).

The average values for coplanarity, BLA and predicted longest wavelength absorption maxima for compounds **11** and **12** were also calculated directly from the geometries adopted in the solid state. Although the values for BLA were almost identical for **11** and **12** (0.069 and 0.066 \AA , respectively), the degree of coplanarity (**11**, 43.02° ; **12**, 11.80°) and consequently the values for λ_{max} (**11**, 354 nm ; **12**, 382 nm) were quite different. The large difference (and perhaps even the unusual all-*syn* conformation adopted by **11**) can be attributed to packing forces in compound **11**. Indeed, intermolecular hydrogen bonding exists between C(5)···H(7B1) (2.6033 \AA) and C(6)···H(7A2) (2.6782 \AA) atoms, giving rise to a polymeric arrangement (see supplementary data†).

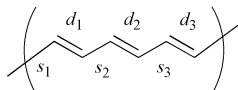
Calculations were performed on the sexithiophene derivatives **9₂**, **11₂** and **12₂**, to determine the effect of chain extension towards structural and electronic properties. There is very little difference in BLA between the three oligomers ($0.009\text{--}0.011\text{ \AA}$), and the degree of conjugation is far higher than in the terthiophene analogues. The planarity within the sexithiophenes

†CCDC reference numbers 158840 and 171910. See <http://www.rsc.org/suppdata/jm/b1/b109017h/> for crystallographic files in .cif or other electronic format.

Table 5 Theoretical and experimental values for bond length alternation, torsion angles and absorption maxima for compounds **9–12**, **9₂**, **11₂** and **12₂**

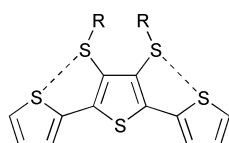
Compound	BLA/Å		Coplanarity ^o		Absorption maximum/nm	
	Calculated	Experimental	Calculated ^a	Experimental	Calculated	Experimental
9	0.030	—	0.02	—	416	360
10	0.025	—	3.69	—	418	368
11 (all- <i>anti</i> conformer)	0.021	—	6.43	—	421	368, 354 ^b
11 (all- <i>syn</i> conformer)	0.036	0.069	16.26	43.02	412	—
12	0.027	0.066	2.27	11.80	421	375, 382 ^c
9₂	0.011	—	2.13	—	503	—
11₂	0.009	—	1.03	—	512	—
12₂	0.010	—	0.84	—	511	—

^aCalculated as an average between adjacent rings. ^bCalculated from the X-ray crystal structure of compound **11**. ^cCalculated from the X-ray crystal structure of compound **12**. The value for BLA in each polyene chain was calculated according to the following equation:


$$\text{BLA} = \frac{[(s_1 - d_1) + (s_2 - d_2) + (s_3 - d_3) + \dots + (s_n - d_n)]}{n}$$

is also generally higher, although **9₂** is less planar than terthiophene **9**. The longest wavelength absorption maxima for **11₂** and **12₂** are similar (512 nm and 511 nm, respectively), but the value for **9₂** is slightly lower at 503 nm, due to a small loss in planarity.

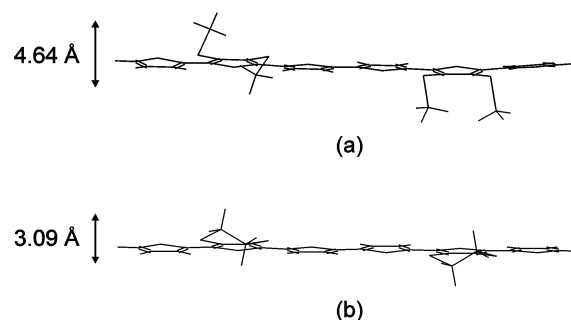
The experimental values for the longest wavelength absorption maxima, obtained from polymer films of poly(**9**), poly(**10**), poly(**11**) and poly(**12**) grown on ITO glass, are relatively similar (478–489 nm, Table 1). Apart from an overestimation in the predicted values (by *ca.* 24 nm), the data are in general agreement with those found experimentally (503–512 nm, Table 5). However, the difference in the optical bandgap values for the polymers is vastly different between those containing linear side chains (poly(**10**), 1.97 eV) and the fused ring analogues (poly(**11**), 1.53 eV; poly(**12**), 1.45 eV). Using Roncali's criteria for the determination of the overall bandgap of a conjugated polymer,⁵² we can exclude some points: the aromatic resonance energy of the thiophene rings and the inductive or resonance effects of the substituents should be almost identical within the series poly(**9–12**). Theoretical calculations and experimental data show that variation in BLA is negligible in the oligothiophene systems. The conformation adopted by the thiophene chain is certain to have an effect upon the bandgap properties of the polymer, but it is generally accepted that the all-*anti* geometry predominates in oligo and polythiophene species. The degree of coplanarity is also an important factor, but it appears from the calculations made on the sexithiophene derivatives (Table 5) that the difference is small and imparts only a small change in the value for λ_{max} . This leads to the conclusion that it must be the intermolecular or intramolecular effects that are causing such an anomaly between the optical bandgaps of the linear and fused ring species. The only intramolecular interactions evident in the terthiophenes or sexithiophenes are between the sulfur atoms of the alkyl substituents and those in the adjacent unsubstituted thiophene ring system (Fig. 11). The average values of intramolecular S...S contacts vary by *ca.* 0.19 Å in the

**Fig. 11** Intramolecular S...S contacts in the all-*anti* terthiophene unit.

terthiophene series (**9**, 2.876 Å; **10**, 2.909 Å; **11**, 2.985 Å; **12**, 2.799 Å) and by *ca.* 0.06 Å for the sexithiophenes (**9₂**, 2.815 Å; **11₂**, 2.852 Å; **12₂**, 2.797 Å). The S...S contacts are marginally closer in the dimers (on average *ca.* 0.06 Å), indicating that extension of the chain length does not have a significant effect on the S...S interactions within the repeat unit. Almost by a process of elimination, the discrepancy between the bandgaps of the linear and fused ring systems must be due to interchain interactions. Undoubtedly, the hexyl chains in poly(**10**) will hinder the approach between chains for efficient π - π stacking or S...S interactions. However, from the UV/vis spectrum (Fig. 10) it appears that the methyl substituents in poly(**9**) also have a similar effect on the resulting bandgap due to steric hindrance. With respect to the alkylthio substituents, the repeat units in poly(**9**) can adopt two different conformations: the two methylsulfanyl groups either in a *cis* or *trans* configuration to the plane of the oligo/polythiophene chain (Fig. 12a). In the case of poly(**11**) (Fig. 12b) or poly(**12**), the conformation of the side chains are restricted due to the more rigid ring system. Therefore, these polymers are more likely to support close interchain π - π or S...S contacts, leading to more extensive intermolecular effects than the linear alkylsulfanyl containing polymers. It is this difference in packing ability that we believe is mainly responsible for the different bandgap properties of the linear and fused ring polythiophenes.

Conclusion

A new series of bis(alkylsulfanyl)terthiophene derivatives (**9–12**) has been prepared. The redox behaviour for compounds

**Fig. 12** Optimised structures of (a) **9₂** and (b) **11₂** showing the possible conformations of the bis(alkylthio) substituents.

possessing linear side-chains (**9** and **10**) and the fused ring derivative **11** is remarkably different. Theoretical calculations show that the HOMOs of terthiophenes bearing linear side groups are stabilised compared to that of **11**, justifying the reduction in the oxidation potential of the latter. The optical and electrochemical properties of the corresponding polymers have been assessed. The longest wavelength absorption maxima are similar for the polymers, although the optical bandgaps are lower for the fused ring polymers. Furthermore, the propensity of poly(**11**) towards p-doping is also superior to poly(**9**), poly(**10**) and poly(**12**), since the former displays two reversible/quasi-reversible oxidation processes (+0.64 and +0.99 V), which are far lower than the single reversible oxidation processes observed in poly(**9**), poly(**10**) and poly(**12**) (at *ca.* +1.2 V). We can conclude that there is a significant advantage to be gained from the use of a cyclic substituent over linear alkylthio side groups and that the redox properties of the ethylene system poly(**11**) are particularly efficient at charge stabilisation.

Reducing the bandgap of conducting polymers by a strategic approach, such as implementing minor modifications in the molecular structure, remains an important goal. Low bandgap materials can be used in a range of optoelectronic devices and we have specifically investigated the possible application of poly(**11**) in plastic solar cells by studying the infrared active vibrations of photodoped poly(**11**). The long-living photo-excited states observed by the photoinduced IR spectrum of poly(**11**) are essential characteristics for use of the material in photovoltaics. Our future progress in this area will involve the bulk chemical polymerisation of **11** and a study into the effect of replacing the ethylenedithio unit with alternative cyclic disulfanyl units.

Experimental

General

Melting points were taken using Electrothermal Melting Point apparatus and are uncorrected. ^1H and ^{13}C NMR spectra were recorded on a Bruker AC 250 instrument; chemical shifts are given in ppm; all J values are in Hz. IR spectra for the characterisation of the compounds were recorded on a Mattson Genesis Series FTIR spectrometer. Mass spectra (EI) and high resolution mass spectra were recorded on a 7070E VG Analytical Mass Spectrometer. Elemental analyses were obtained by MEDAC Ltd.

Crystal structure determination of **11** and **12**[†]

Data were collected on a Nonius Kappa CCD area detector diffractometer with a rotating anode following standard procedures.^{30,42}

Cyclic voltammetry

The measurements for compounds **9**, **10**, **11** and **12** were performed on a BAS CV50W voltammetric analyser with iR compensation, using anhydrous acetonitrile as the solvent, aqueous Ag/AgCl as the reference electrode and platinum wire and gold disk as the counter and working electrodes, respectively. All solutions were degassed (N_2) and contained the substrate in concentrations *ca.* 10^{-3} M, together with $n\text{-Bu}_4\text{NPF}_6$ (0.1 M) as the supporting electrolyte. Electro-polymerisation experiments were conducted in dichloromethane or acetonitrile, using a gold disk or ITO glass working electrode. Voltammograms of the as-grown polymer films were recorded in anhydrous acetonitrile using aqueous Ag/AgCl as the reference electrode and platinum wire as the counter electrode.

FTIR Spectroscopy: *in-situ* spectroelectrochemistry and photoinduced absorption

Attenuated total reflection FTIR spectroelectrochemistry was performed *in situ* using the set-up described elsewhere.⁵⁴ A Pt grid evaporated onto a ZnSe reflection element was the working electrode while a Pt foil and a Ag/AgCl wire were the counter and the quasi-reference electrode, respectively (for the sake of clarity all potential values refer to the aqueous Ag/AgCl electrode). The electrolyte solution was 0.1 M $n\text{-Bu}_4\text{NPF}_6$ in anhydrous acetonitrile. Infrared spectra were recorded consecutively during a potential sweep at a rate of 5 mV s^{-1} . Specific spectral changes related to the electrochemical process were obtained by comparing subsequent spectra to the spectrum recorded under an applied potential of 100 mV. Spectra are calculated as $\Delta(-\log T_{\text{ATR}})$, where T_{ATR} is the transmission in the ATR geometry, and each of them covers about 90 mV in the cyclic voltammogram. For photoinduced IR absorption, the as-grown polymer films were kept under an applied potential of -700 mV until no current was detectable, rinsed with fresh acetonitrile and then dried in an argon laminar flow box. The samples were placed in a liquid N_2 bath cryostat with ZnSe windows and illuminated in 45° geometry by the 488 nm line of an Ar^+ laser (22 mW cm^{-2}). The photoinduced changes in the infrared absorption spectrum were measured by collecting 300 repetitions of 10 co-added single beam spectra recorded under illumination and of 10 co-added single beam spectra recorded in the dark. Combining the correspondent light-on and dark spectra, the photoinduced absorption was calculated as $-\Delta T/T$. During measurements, the vacuum was better than 10^{-5} mbar. Doping induced and photoinduced FTIR spectra were recorded with a resolution of 4 cm^{-1} , using a Bruker IFS 66S spectrometer equipped with a liquid N_2 cooled MCT detector.

4,5-Di(2-thenoyl)-1,3-dithiol-2-one (**14**)

To a solution of **13** (3.36 g, 9.49 mmol) in dichloromethane-glacial acetic acid (3 : 1 v/v) was added mercuric acetate (4.84 g, 0.152 mmol). The mixture was stirred at room temperature for 16 h, filtered and washed with dichloromethane (50 ml). The organic extracts were washed with copious amounts of water and saturated sodium bicarbonate solution, then dried (MgSO_4). The solvent was removed under reduced pressure to afford **14** as a pale yellow solid (2.45 g, 76%), mp $130\text{--}132^\circ\text{C}$ (Found: C, 45.76; H, 1.73. Calcd for $\text{C}_{13}\text{H}_6\text{O}_3\text{S}_4$: C, 46.13; H, 1.79%; ^1H NMR (CDCl_3) δ /ppm 7.71 (2 H, dd, $J = 0.8$ and 5.46), 7.69 (2 H, dd, $J = 0.88$ and 4.04), 7.09 (2 H, m); $\nu_{\text{max}}/\text{cm}^{-1}$ 2173, 1623, 1506, 1405, 1268, 1110 and 1045; HRMS (EI) calcd for $\text{C}_{13}\text{H}_6\text{O}_3\text{S}_4$ 337.91998, found 337.91693.

4,6-Di(2-thienyl)thieno[3,4-*d*]-1,3-dithiol-2-one (**15**)

A mixture of **14** (1 g, 2.95 mmol), P_2S_5 (3.2 g, 13.7 mmol) and NaHCO_3 (1 g) in 1,4-dioxane (20 ml) was stirred under dry nitrogen whilst the temperature was raised from $60\text{--}90^\circ\text{C}$ over 1 h. The mixture was cooled, water was added (150 ml) (CAUTION! H_2S and CO_2 evolution) and the suspension was allowed to reflux for 0.5 h. Upon cooling, the crude product was filtered, washed with water (50 ml) and dried *in vacuo*. The product was isolated by column chromatography (silica, petroleum spirit $40\text{--}60^\circ\text{C}$ with gradual change to dichloromethane) to afford **15** as a light orange solid (0.63 g, 63%), mp $170\text{--}172^\circ\text{C}$; ^1H NMR (CDCl_3) δ /ppm 7.39, (2 H, dd, $J = 0.96$ and 4.52), 7.24 (2 H, dd, $J = 0.95$ and 3.61), 7.12 (2 H, m); $\nu_{\text{max}}/\text{cm}^{-1}$ 2361, 1653, 840 and 700; HRMS (EI) calcd for $\text{C}_{13}\text{H}_6\text{O}_5$ 337.90222, found 337.90107.

2,5-Di(2-thienyl)-3,4-bis(2-cyanoethylsulfanyl)thiophene (16)

A solution of compound **15** (0.75 g, 2.22 mmol) in dry tetrahydrofuran (30 ml) under dry nitrogen was cooled to 0 °C. Potassium *tert*-butoxide (0.58 g, 4.87 mmol) was added and the mixture was allowed to stir at 0 °C for 1 h. 3-Bromopropionitrile (0.41 ml, 4.87 mmol) was added and this was allowed to stir under dry nitrogen for approximately 2 h whilst warming to room temperature. The reaction was poured into water (50 ml) and the product was extracted into ethyl acetate (3 × 50 ml). The combined organic extracts were washed with water (2 × 100 ml) and dried (MgSO₄). The solvent was removed under reduced pressure and the product was isolated by column chromatography (silica, dichloromethane), to afford **16** as a dark orange solid (0.65 g, 70%), mp 132–134 °C (Found: C, 51.15; H, 3.65; N, 6.70; S, 38.02. Calcd for C₁₈H₁₄N₂S₅: C, 51.64; H, 3.37; N, 6.69; S, 38.30%); $\nu_{\max}/\text{cm}^{-1}$ 2219, 1473, 1409, 1052, 840, 821, 728 and 709; ¹H NMR (CDCl₃) δ /ppm 7.49 (2 H, dd, *J* = 0.97 and 3.62), 7.43 (2 H, dd, *J* = 0.94 and 5.15), 7.11 (2 H, m), 3.12 (4 H, t, *J* = 7.31), 2.58 (4 H, t, *J* = 7.35); HRMS (EI) calcd for C₁₈H₁₄S₅N₂ 417.97604, found 417.97845.

General procedure for compounds 9–12

To a solution of **16** in dry tetrahydrofuran (50 ml) at 0 °C under dry nitrogen was added tetrabutylammonium hydroxide (1 M solution in methanol, 2.2 equivalents). The reaction was allowed to stir at this temperature for 1 h at which time the corresponding alkyl halide was added (2.2 equivalents). The reaction was allowed to warm to room temperature and was stirred for a further 3 h. Water was added (100 ml) and the product was extracted into ethyl acetate (3 × 75 ml). The combined organic extracts were washed with water (2 × 100 ml) and dried (MgSO₄). The products were isolated by column chromatography (silica, dichloromethane).

2,5-Di(2-thienyl)-3,4-bis(methylsulfanyl)thiophene (9). From **16** (200 mg, 0.48 mmol), **9** was afforded as a green-yellow solid (85 mg, 52%), mp 42–44 °C (Found: C, 49.49; H, 3.59; S, 46.35. Calcd for C₁₄H₁₂S₅: C, 49.37; H, 3.55; S, 47.08%); ¹H NMR (CDCl₃) δ /ppm 7.46 (2 H, dd, *J* = 1.33 and 4.29), 7.38 (2 H, dd, *J* = 1.10 and 5.13), 7.07 (2 H, m), 2.4 (6 H, s); $\nu_{\max}/\text{cm}^{-1}$ 1411, 1056, 835 and 686; HRMS (EI) calcd for C₁₄H₁₂S₅ 339.95425, found 339.95578.

2,5-Di(2-thienyl)-3,4-bis(hexylsulfanyl)thiophene (10). From **16** (120 mg, 0.36 mmol), **10** was obtained as a dark orange oil (90 mg, 53%), ¹H NMR (CDCl₃) δ /ppm 7.45 (2 H, d, *J* = 3.95), 7.39 (2 H, d, *J* = 4.87), 7.07 (2 H, m), 2.9 (4 H, t, *J* = 7.25), 1.6 (4 H, m), 1.3 (12 H, m), 0.9 (6 H, t, *J* = 6.59); HRMS (EI) calcd for C₂₄H₃₂S₅ 480.11075, found 480.11060.

2,5-Di(2-thienyl)-3,4-(ethylenedisulfanyl)thiophene (11). From **16** (250 mg, 0.60 mmol) **11** was obtained as a pale yellow solid (120 mg, 59%), mp 140–142 °C (Found: C, 49.85; H, 3.03. Calcd for C₁₄H₁₀S₅: C, 49.67; H, 2.98%); ¹H NMR (CDCl₃) δ /ppm 7.35 (2 H, d, *J* = 1.15), 7.32 (2 H, d, *J* = 1.56), 7.09 (2 H, m), 3.28 (4 H, s); HRMS (EI) calcd for C₁₄H₁₀S₅ 337.93860, found 337.93731.

2,5-Di(2-thienyl)-3,4-(propylenedisulfanyl)thiophene (12). From **16** (300 mg, 0.71 mmol) **12** was obtained as an orange solid (170 mg, 68%), mp 134–136 °C (Found: C, 51.23; H, 3.41; S, 46.07. Calcd for C₁₅H₁₂S₅: C, 51.10; H, 3.43; S, 45.47%); ¹H NMR (CDCl₃) δ /ppm 7.32 (2H, dd, *J* = 1.10 and 3.71), 7.28 (2H, dd, *J* = 1.17 and 5.15), 6.99 (2H, dd, *J* = 3.64 and 5.15), 2.77 (4H, br s) and 2.36 (2H, br s); EIMS (M⁺) 352.

References

- 1 S. J. Higgins, *Chem. Soc. Rev.*, 1997, **26**, 247.
- 2 (a) G. Tourillon and F. Garnier, *J. Phys. Chem.*, 1983, **87**, 2289; (b) R. J. Waltman, J. Bargon and A. F. Diaz, *J. Phys. Chem.*, 1983, **87**, 1459.
- 3 J. H. Schon, A. Dodabalapur, Z. Bao, C. Kloc, O. Schenker and B. Batlogg, *Nature*, 2001, **410**, 189.
- 4 J. Roncali, *Chem. Rev.*, 1992, **92**, 711 and references therein.
- 5 J. Roncali, F. Garnier, R. Garreau and M. Lemaire, *J. Chem. Soc., Chem. Commun.*, 1987, 1500.
- 6 L. B. Groenendaal, F. Jonas, D. Freitag, H. Pielartzik and J. R. Reynolds, *Adv. Mater.*, 2000, **12**, 481.
- 7 G. Gourillon and F. Garnier, *J. Electroanal. Chem.*, 1984, **161**, 51.
- 8 R. L. Elsenbaumer, K. Y. Jen and R. Oobodi, *Synth. Met.*, 1986, **15**, 169.
- 9 S. Tanaka, M. Sato and K. Kaeriyama, *Synth. Met.*, 1988, **25**, 277.
- 10 J. P. Ruiz, K. Nayak, D. S. Marynick and J. R. Reynolds, *Macromolecules*, 1989, **22**, 1231.
- 11 X. Wu, T.-A. Chen and R. D. Rieke, *Macromolecules*, 1995, **28**, 2101.
- 12 F. Goldoni, D. Iarossi, A. Mucci, L. Schenetti and M. Zambianchi, *J. Mater. Chem.*, 1997, **7**, 593.
- 13 F. Goldoni, R. A. J. Janssen and E. W. Meijer, *J. Polym. Sci. A: Polym. Chem.*, 1999, **37**, 4629.
- 14 C. Wang, J. L. Schindler, C. R. Kannewurf and M. G. Kanatzidis, *Chem. Mater.*, 1995, **7**, 58.
- 15 G. A. Sotzing and J. R. Reynolds, *Chem. Mater.*, 1996, **8**, 882.
- 16 Y. Fu, H. Cheng and R. L. Elsenbaumer, *Chem. Mater.*, 1997, **9**, 1720.
- 17 J. C. Carlberg and O. Inganäs, *J. Electrochem. Soc.*, 1997, **144**, L61.
- 18 M. C. Morvant and J. R. Reynolds, *Synth. Met.*, 1998, **92**, 57.
- 19 L. Huchet, S. Akoudad and J. Roncali, *Adv. Mater.*, 1998, **10**, 541.
- 20 S. Akoudad and J. Roncali, *Synth. Met.*, 1998, **93**, 111.
- 21 A. Lima, P. Schottland, S. Sadki and C. Chevrot, *Synth. Met.*, 1998, **93**, 33.
- 22 O. Stéphane, P. Schottland, P.-Y. Le Gall, C. Chevrot, C. Mariet and M. Carrier, *J. Electroanal. Chem.*, 1998, **443**, 217.
- 23 H. Randriamahazaka, V. Noël and C. Chevrot, *J. Electroanal. Chem.*, 1999, **472**, 103.
- 24 S. Akoudad and J. Roncali, *Electrochem. Commun.*, 2000, **2**, 72.
- 25 D. Iarossi, A. Mucci, L. Schenetti, R. Seeber, F. Goldoni, M. Affronte and F. Nava, *Macromolecules*, 1999, **32**, 1390.
- 26 S. C. Ng and P. Miao, *Macromolecules*, 1999, **32**, 5313.
- 27 C. Wang, M. E. Benz, E. LeGoff, J. L. Schindler, J. Allbritton-Thomas, C. R. Kannewurf and M. G. Kanatzidis, *Chem. Mater.*, 1994, **6**, 401.
- 28 Preliminary communication: C. Pozo-Gonzalo, D. M. Roberts and P. J. Skabara, *Synth. Met.*, 2001, **119**, 115.
- 29 P. J. Skabara, I. M. Serebryakov, D. M. Roberts, I. F. Perepichka, S. J. Coles and M. B. Hursthouse, *J. Org. Chem.*, 1999, **64**, 6418.
- 30 Crystal data for compound **11**: C₁₄H₁₀S₅, *M*_r = 338.52, *T* = 150(2) K, orthorhombic, space group *Cmc*2₁, *a* = 20.6948(7), *b* = 8.7890(3), *c* = 7.7472(3) Å, *V* = 1409.11(9) Å³, ρ_{calc} = 1.596 g cm⁻³, μ = 0.803 mm⁻¹, *Z* = 4, reflections collected: 6285, independent reflections: 1246 (*R*_{int} = 0.0276), final *R* indices [*I* > 2 σ (*I*): *R*₁ = 0.0224, *wR*₂ = 0.0579, *R* indices (all data): *R*₁ = 0.0231, *wR*₂ = 0.0583.
- 31 See for example: S. Golhen, L. Ouahab, A. Lebeuze, M. Bouayed, P. Delhaes, Y. Kashimura, R. Kato, L. Binet and J.-M. Fabre, *J. Mater. Chem.*, 1999, **9**, 387.
- 32 Cambridge Data Base: F. H. Allen, O. Kennard and R. Taylor, *Acc. Chem. Res.*, 1983, **16**, 146–153.
- 33 Q. Minxie, C. Yong, F. Heng, T. Youqi and Z. Fugui, *Acta Phys. Chim. Sin.*, 1990, **6**, 277.
- 34 L. DeWitt, G. J. Blanchard, E. LeGoff, M. E. Benz, J. H. Liao and M. G. Kanatzidis, *J. Am. Chem. Soc.*, 1993, **115**, 12158.
- 35 G. Barbarella, M. Zambianchi, A. Bongini and L. Antolini, *Adv. Mater.*, 1994, **6**, 561.
- 36 J. P. Ferraris, A. Bravo, W. Kim and D. C. Hrnecir, *J. Chem. Soc., Chem. Commun.*, 1994, 991.
- 37 (a) D. D. Graf, J. P. Campbell, L. L. Miller and K. R. Mann, *J. Am. Chem. Soc.*, 1996, **118**, 5480; (b) D. D. Graf, R. G. Duan, J. P. Campbell, L. L. Miller and K. R. Mann, *J. Am. Chem. Soc.*, 1997, **119**, 5888.
- 38 P. A. Chaloner, S. R. Gunatunga and P. B. Hitchcock, *J. Chem. Soc., Perkin Trans. 2*, 1997, 1597.
- 39 T. M. Barclay, A. W. Cordes, C. D. McKinnon, R. T. Oakley and R. W. Reed, *Chem. Mater.*, 1997, **9**, 981.
- 40 D. H. Kim, B. S. Khan, S. M. Lim, K.-M. Bark, B. G. Kim,

- M. Shiro, Y.-B. Shim and S. C. Shin, *J. Chem. Soc., Dalton Trans.*, 1998, 1893.
- 41 O. Clot, M. O. Wolf and B. O. Patrick, *J. Am. Chem. Soc.*, 2000, **122**, 10456.
- 42 Crystal data for compound **12**: C₁₅H₁₂S₅, $M_r = 352.55$, $T = 150(2)$ K, orthorhombic, space group *Pbca*, $a = 15.721(3)$, $b = 8.860(2)$, $c = 21.597(4)$ Å, $V = 3008.2(10)$ Å³, $\rho_{\text{calc}} = 1.557$ g cm⁻³, $\mu = 0.755$ mm⁻¹, $Z = 8$, reflections collected: 14827, independent reflections: 3385 ($R_{\text{int}} = 0.0400$), final R indices [$I > 2\sigma I$]: $R_1 = 0.0337$, $wR_2 = 0.0768$, R indices (all data): $R_1 = 0.0508$, $wR_2 = 0.0854$.
- 43 (a) Gaussian 98, Revision A.7, M. J. Frisch, G. W. Trucks, H. B. Schlegel, G. E. Scuseria, M. A. Robb, J. R. Cheeseman, V. G. Zakrzewski, J. A. Montgomery Jr., R. E. Stratmann, J. C. Burant, S. Dapprich, J. M. Millam, A. D. Daniels, K. N. Kudin, M. C. Strain, O. Farkas, J. Tomasi, V. Barone, M. Cossi, R. Cammi, B. Mennucci, C. Pomelli, C. Adamo, S. Clifford, J. Ochterski, G. A. Petersson, P. Y. Ayala, Q. Cui, K. Morokuma, D. K. Malick, A. D. Rabuck, K. Raghavachari, J. B. Foresman, J. Cioslowski, J. V. Ortiz, A. G. Baboul, B. B. Stefanov, G. Liu, A. Liashenko, P. Piskorz, I. Komaromi, R. Gomperts, R. L. Martin, D. J. Fox, T. Keith, M. A. Al-Laham, C. Y. Peng, A. Nanayakkara, C. Gonzalez, M. Challacombe, P. M. W. Gill, B. Johnson, W. Chen, M. W. Wong, J. L. Andres, C. Gonzalez, M. Head-Gordon, E. S. Replogle and J. A. Pople, Gaussian, Inc., Pittsburgh, PA, 1998.
- 44 (a) See for example: G. Zerbi, M. Gussoni and C. Castiglioni, in *Conjugated Polymers*, ed. J. L. Brédas and R. Silbey, Kluwer, Dodrecht, 1991, p. 435; (b) M. Del Zoppo, C. Castiglioni, P. Zuliani and G. Zerbi, in *Handbook of Conducting Polymers*, 2nd edn., ed. T. A. Skotheim and J. R. Reynolds, Marcel Dekker, New York, 1988, ch. 28 and references therein.
- 45 (a) B. Horovitz, *Solid State Commun.*, 1982, **41**, 729; (b) E. Ehrenfreund, Z. V. Vardeny, O. Brafman and B. Horowitz, *Phys. Rev. B*, 1987, **36**, 1535.
- 46 E. Ehrenfreund and Z. V. Vardeny, *Proc. SPIE – Int. Soc. Opt. Eng.*, 1997, **3145**, 324.
- 47 (a) G. Yu, J. Gao, J. C. Hummelen and F. Wudl, *Science*, 1995, **258**, 1474; (b) C. J. Brabec, F. Padinger, N. S. Sariciftci and J. C. Hummelen, *J. Appl. Phys.*, 1999, **85**, 6866.
- 48 A. Cravino, H. Neugebauer, S. Luzzati, M. Catellani and N. S. Sariciftci, *J. Phys. Chem. B*, 2001, **105**, 46.
- 49 B. Tian, G. Zerbi and K. Mueller, *J. Chem. Phys.*, 1991, **95**, 3198.
- 50 H. Neugebauer, C. Kvarnström, A. Cravino, T. Yohannes and N. S. Sariciftci, *Synth. Met.*, 2001, **116**, 115.
- 51 M. Gussoni, C. Castiglioni and G. Zerbi, in *Spectroscopy of Advanced Materials*, eds. R. J. H. Clark and R. E. Hester, Wiley, New York, 1991, p. 251.
- 52 J. Roncali, *Chem. Rev.*, 1997, **97**, 173.
- 53 Data were obtained from semi-empirical calculations at the PM3 level, using the Hyperchem software package.
- 54 (a) H. Neugebauer, *Macromol. Symp.*, 1995, **94**, 61; (b) Z. Ping, H. Neugebauer and A. Neckel, *Electrochim. Acta*, 1996, **41**, 767; (c) H. Neugebauer and Z. Ping, *Mikrochim. Acta [Suppl.]*, 1997, **14**, 125.